East Antarctic ice sheet most vulnerable to Weddell Sea warming

N. R. Golledge[1,2] (ID)**, R. H. Levy[2]** (ID)**, R. M. McKay[1]** (ID)**, and T. R. Naish[1]** (ID)

[1] Antarctic Research Centre, Victoria University of Wellington, Wellington, New Zealand, [2] GNS Science, Lower Hutt, New Zealand

Abstract Models predict considerable spatial variability in the magnitude of future climate change around Antarctica, suggesting that some sectors of the continent may be more affected by these changes than others. Furthermore, the geometry of the bedrock topography underlying the East and West Antarctic ice sheets, together with regional differences in ice thickness, mean that certain ice drainage basins may respond more or less sensitively to environmental forcings. Here we use an ensemble of idealized climates to drive ice-sheet simulations that explore regional and continental-scale thresholds, allowing us to identify a hierarchy of catchment vulnerabilities based on differences in long-term catchment-averaged ice loss. Considering this hierarchy in the context of recent observations and climate scenarios forecast for 2100 CE, we conclude that the majority of future ice loss from East Antarctica, both this century and over subsequent millennia, will likely come from the Recovery subglacial basin in the eastern Weddell Sea.

1. Introduction

Climate model simulations for the present century indicate that significant oceanic and atmospheric warming is likely unless current greenhouse gas emission levels are substantially reduced [*Collins et al.*, 2013]. The impact that such environmental change may have on Antarctic ice sheets has been the subject of several recent studies [*Ritz et al.*, 2015; *Golledge et al.*, 2015; *DeConto and Pollard*, 2016], which although contrasting in the magnitude of ice loss they predict, all agree that over centennial timescales, sea-level contributions of several meters are possible. In these simulations, however, the majority of ice loss is from the marine-based West Antarctic Ice Sheet (WAIS). The response of the East Antarctic Ice Sheet (EAIS) to environmental warming is harder to predict because the ice sheet covers a much larger area than the WAIS and has a bedrock topography characterized both by deep subglacial basins and by high, buried, mountain ranges [*Fretwell et al.*, 2013]. Recent studies show that areas of the EAIS such as the Filchner Ice Shelf (Recovery Catchment) and Totten Ice Shelf (Aurora Catchment) are already experiencing southward flux of warm ocean water [*Darelius et al.*, 2016; *Rintoul et al.*, 2016], and thus, an imperative exists to examine likely ice sheet responses in these, and other, regions. One complication is that the timescale of EAIS response is likely to be significantly longer than that of the WAIS, due to generally slower flow of East compared to West Antarctic glaciers [*Rignot et al.*, 2011] and the longer transit times that are associated with the much larger EAIS. To investigate this, we run multimillennial simulations using a three-dimensional ice sheet model that is capable of simulating sheet, stream, and shelf flow. Specifically, we investigate how the interplay between ocean forcing, atmospheric forcing, and topographic stabilization affects long-term mass loss patterns at the catchment scale. By employing a range of idealized ocean and atmosphere warming scenarios, we quantify long-term ice sheet responses and identify whether or not distinct climate ice sheet thresholds exist.

2. Methods

Our modeling procedure closely follows an established protocol refined through previous experimentation [*Golledge et al.*, 2015; *Aitken et al.*, 2016; *Golledge et al.*, 2016]. We use the Parallel Ice Sheet Model v.0.6.3 [*Bueler and Brown*, 2009] which solves equations of the shallow-ice and shallow-shelf approximations (SIA and SSA, respectively). Both SIA and SSA are used in the derivation of grounded ice velocities, whereas only the SSA is used for floating ice [*Bueler and Brown*, 2009]. Combining SIA and SSA velocity solutions for grounded ice allows basal sliding to be simulated as a "dragging shelf" and enables the stress regime across the grounding line to be treated in a continuous manner [*Winkelmann et al.*, 2010]. Plastic failure of saturated basal till

[*Schoof*, 2006] allows ice streams to develop naturally wherever the thermal regime facilitates the production of basal meltwater. We use a model grid of 20 km in order to enable a large number of simulations to be undertaken. Although mesh resolution can lead to differing outcomes in some cases [*Martin et al.*, 2015], we have found in previous experiments that this is not the case for our implementation [*Golledge et al.*, 2015], perhaps as a consequence of the unavoidable bed smoothing that occurs during the multistage spin-up procedure or because of the resolution-specific stress balance tuning that is employed. Furthermore, our principal aim here is not so much to define absolute ice geometries as to identify differences between scenarios, for which we believe our approach to be both suitable and robust.

Migration of glacier grounding lines is a fundamental requirement for Antarctic ice sheet simulations, but its implementation remains much debated. Here we use a grounding-line scheme that uses a subgrid interpolation scheme to improve the accuracy of grounding line movements [*Feldmann et al.*, 2014]. The method uses a subgrid interpolation of basal driving stress together with the calculation of one-sided derivatives to better characterize the ice sheet/shelf junction. In the simulations presented here the subgrid scheme is not used to interpolate basal melt, however, meaning that subshelf melt rates are applied only to fully floating cells and are not extended landward to affect a portion of the first upstream grounded cell. The difference between this implementation and the subgrid basal melt interpolation is that the former, as used here, tends to produce slower grounding-line retreat than the latter [cf. *Golledge et al.*, 2015]. Subshelf melt is calculated using a boundary layer thermodynamics approach following *Hellmer et al.* [1998]; *Holland and Jenkins* [1999]. This scheme calculates the freezing point in the boundary layer from pressure (i.e., depth) and salinity and subsequently derives melt rates from energy and salt flux gradients. Different approximations of the temperature at the ice shelf base are used depending on whether there is melt, freeze on, or neither. This scheme has been used previously in Antarctic ice sheet simulations [*Mengel and Levermann*, 2014], but we acknowledge that a different method for calculating melt rates could produce different results.

We drive our model simulations with monthly climatological variations based on present-day data [*Comiso*, 2000; *Lenaerts et al.*, 2012] and use a positive degree-day (PDD) model to calculate and track snow thickness and to allow for melting of snow and ice at 3 and 8 mm/°C/d, respectively where air temperatures are above freezing. The PDD scheme also incorporates a normally distributed, mean zero, white noise signal in the calculation of daily temperature fluctuations. We set the standard deviation of daily temperature variability at 2°C on the basis that the commonly used value of 5°C tends to overestimate surface melting [*Seguinot*, 2013; *Rogozhina and Rau*, 2014]. Retention of a proportion of meltwater within the extant snowpack is parameterized with a refreezing coefficient of 0.6, although this number is not well constrained. Our ensemble of climate scenarios uses the above formulation as a starting point, to which we add a spatially uniform increment in oceanic and/or atmospheric temperatures. Because precipitation rates are closely tied to atmospheric temperatures [*Frieler et al.*, 2015] we incorporate a temperature-dependent precipitation change of 5.3% K^{-1} air temperature anomaly [*Golledge et al.*, 2015]. All experiments that involve a modified atmospheric forcing therefore also implicitly include a perturbed hydrological cycle. All results are compared to a control scenario in which ocean and atmospheric perturbations above present are set to zero.

3. Results

Our model ensemble consists of six ocean temperature and seven air temperature scenarios, which after the 10,000 year long model run result in 42 individual ice-sheet geometries (Figure S1). This lengthy simulation is designed to allow the long response timescale of the EAIS to be captured. This ensures that our results are not affected by any short-term changes related to initial model conditions, and instead reflect a near-equilibrium response of the ice sheet. We define 'near-equilibrium' as a state in which the ice sheet is dynamic and subject to stochastic mass changes as a consequence of climatological variability, but which exhibits a more-or-less constant rate of mass change that is close to zero (Figure S6).

This suite of idealized climatology simulations illustrates the theoretical dependency of both East and West Antarctic ice sheets on environmental conditions. Figures S1 and S2 illustrate the sensitivity of West Antarctic marine-based ice to oceanic conditions, regardless of the air temperature anomaly. In our experiments, marine-based sectors of West Antarctica remain stable even after 10,000 years if oceanic temperatures remain below 0.5°C above present values but collapse when this threshold is exceeded. Atmospheric forcing has a more complex and spatially variable influence, however. To better understand whether these ice sheet reorganizations are linearly related to climate, or governed by thresholds, we isolate the sea-level equivalent
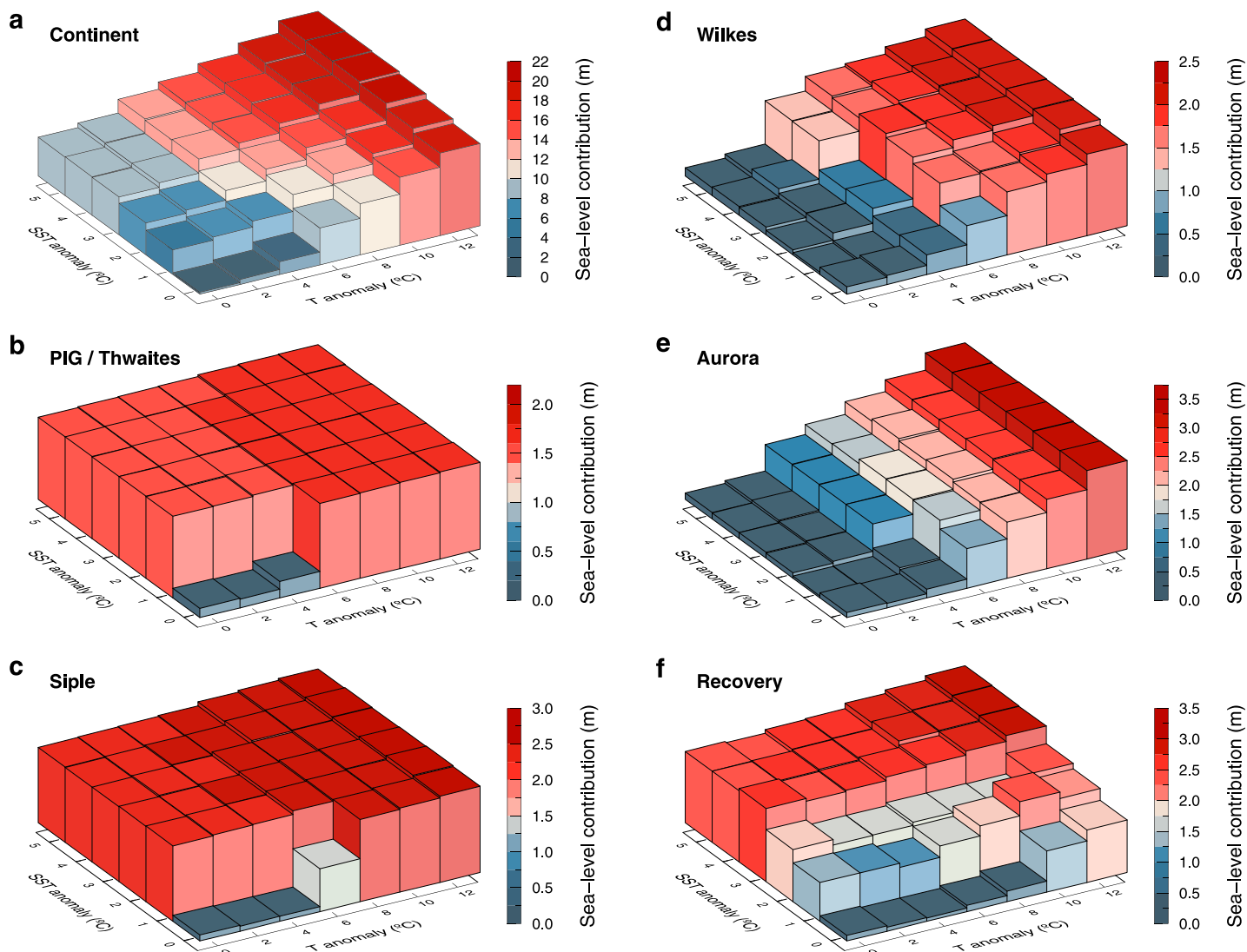
Figure 1. (a) Continent-wide sea-level contributions after 10,000 model years. (b–f) Sea-level contributions from five discrete drainage basins, showing considerable differences in environmental sensitivity and nature of threshold response under warmer-than-present air (T) and ocean (SST) temperatures. The Pine Island Glacier (PIG)/Thwaites Glacier and Siple Coast catchments of West Antarctica (Figures 1b and 1c) exhibit high sensitivity to relatively modest warming values; Wilkes (Figure 1d) and Aurora (Figure 1e) catchments exhibit a threshold sensitivity to air temperature, but not ocean temperature; Recovery basin (Figure 1f) exhibits an abrupt response to ocean temperature but is less sensitive to air temperature.

ice volume change for five of the largest Antarctic catchments for each temperature combination and compare them to the continentally integrated response pattern (Figure 1). What is clear from this representation is that, at the continental scale, ice loss tends to increase more or less linearly with increasing oceanic and atmospheric temperatures (Figure 1a). However, sectoral behaviors are markedly different, with WAIS catchments (Pine Island Glacier/Thwaites Glacier and the Siple Coast) displaying a clear and abrupt sensitivity to ocean temperature that yields almost uniform magnitudes of ice loss once a threshold of 1°C ocean warming is imposed. This is not the case for the Wilkes and Aurora catchments of East Antarctica, however, whose response is near zero under all applied ocean warming perturbations in which atmospheric warming is below 4°C. Above this atmospheric threshold, ice loss appears to increase linearly with rising air temperature, but varies to a lesser degree with increases in oceanic temperature. If these four catchments (Figures 1b–1e) define "typical" West and East Antarctic ice sheet responses, respectively, the behavior shown by the Recovery Catchment appears to exhibit elements of both east and west characteristics. The response profile of the Recovery Catchment (Figure 1f) shows a greater dependency on oceanic temperatures than the other two East Antarctic catchments yet has a less abrupt threshold than seen in the two West Antarctic examples.
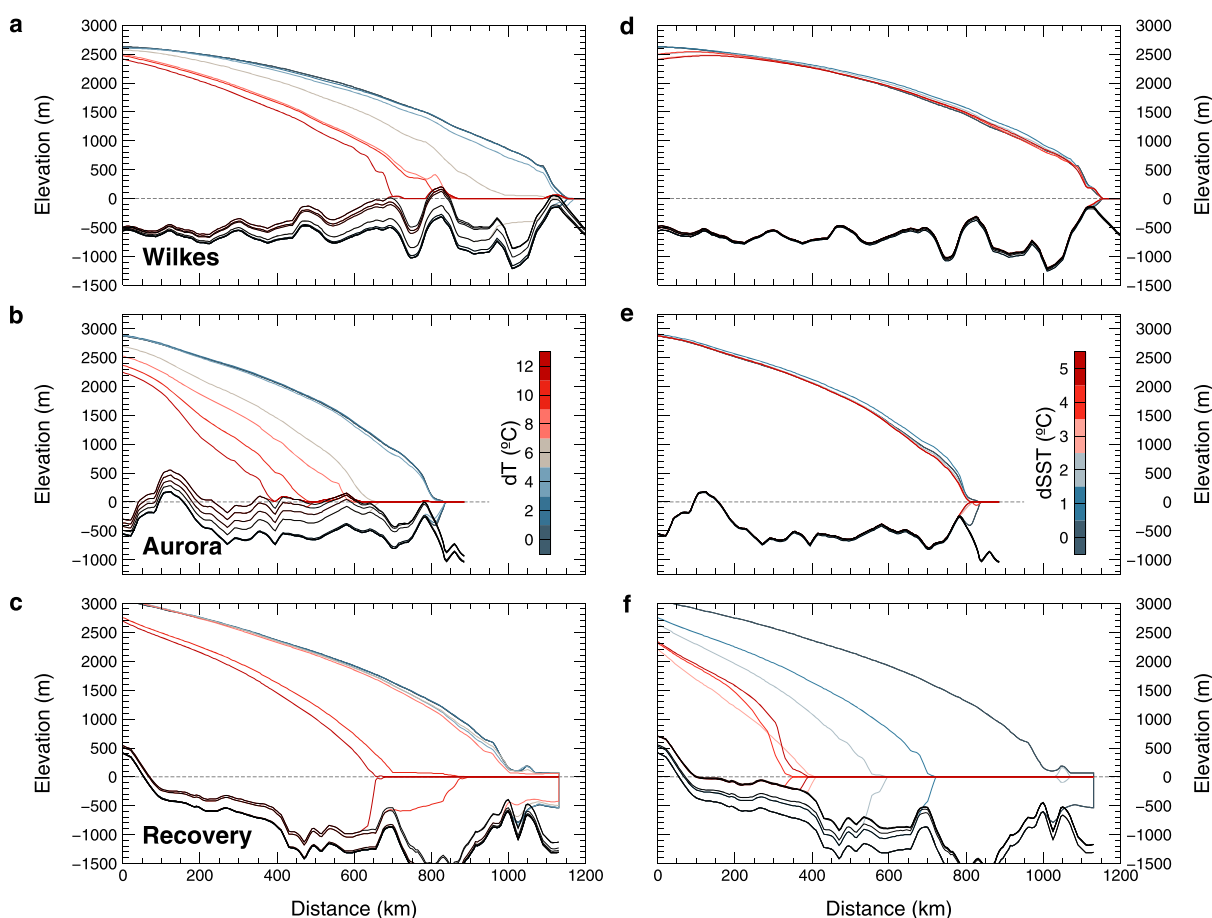
Figure 2. Transects through three major East Antarctic drainage basins after 10,000 model years (see Figure S2 for locations). (a–c) All three investigated sectors of East Antarctica respond to atmospheric warming by retreating inland. However, the magnitude of warming required to initiate retreat, as well as the rate of recession, are dictated by local topography and ice sheet configuration. (d–f) In the absence of atmospheric warming, only Recovery Glacier retreats in response to a warming ocean. Glaciers in both Wilkes and Aurora subglacial basins remain stable due to the greater thickness of ice above flotation at their present-day grounding lines. Panels also show bedrock uplift following ice retreat.

The response of the three major East Antarctic drainage basins shown in Figure 1 reveals that, despite common environmental forcings, the glaciological response is modulated by an additional factor. Investigating this in more detail we extract ice geometries along individual transects through each of the three East Antarctic basins. To simplify the process of attribution, we focus on ocean warming scenarios in which air temperatures remain unchanged and on atmospheric warming experiments in which ocean temperatures do not change. Although the resultant climatologies may not necessarily reflect realistic climate change scenarios, the ice sheet profiles that result provide useful insights into the nature of the additional control that modulates the applied climate forcings. Figures 2a–2c illustrate that, in the absence of ocean warming, ice surface lowering from rising air temperatures and increased surface melting affects all three catchments in a similar manner. By contrast, the same ice margins respond very differently when forced only by a warming ocean (Figure 2d–f). In this case, ice in the Wilkes and Aurora subglacial basins appears inert with respect to warming of the adjacent ocean, yet identical perturbations in the Recovery Catchment (Figure 2f) lead to substantial ice loss and grounding-line retreat.

The reason for the marked differences in response within the three East Antarctic basins is that the ice sheet is underpinned by a topographic high point at the seaward margin of both Wilkes and Aurora basins, yet in the Recovery, the margin is grounded well below sea level and terminates in a floating ice shelf. This configuration leads to a greater volume of ice at the Recovery grounding line that is closer to flotation than in the other two catchments; thus, rendering the catchment as a whole more susceptible to thermal erosion by warmer water. A corollary of this configuration is that the loss of relatively "thin" ice in Recovery, compared to the Wilkes and Aurora, leads to significantly less isostatic rebound which could help to stabilize
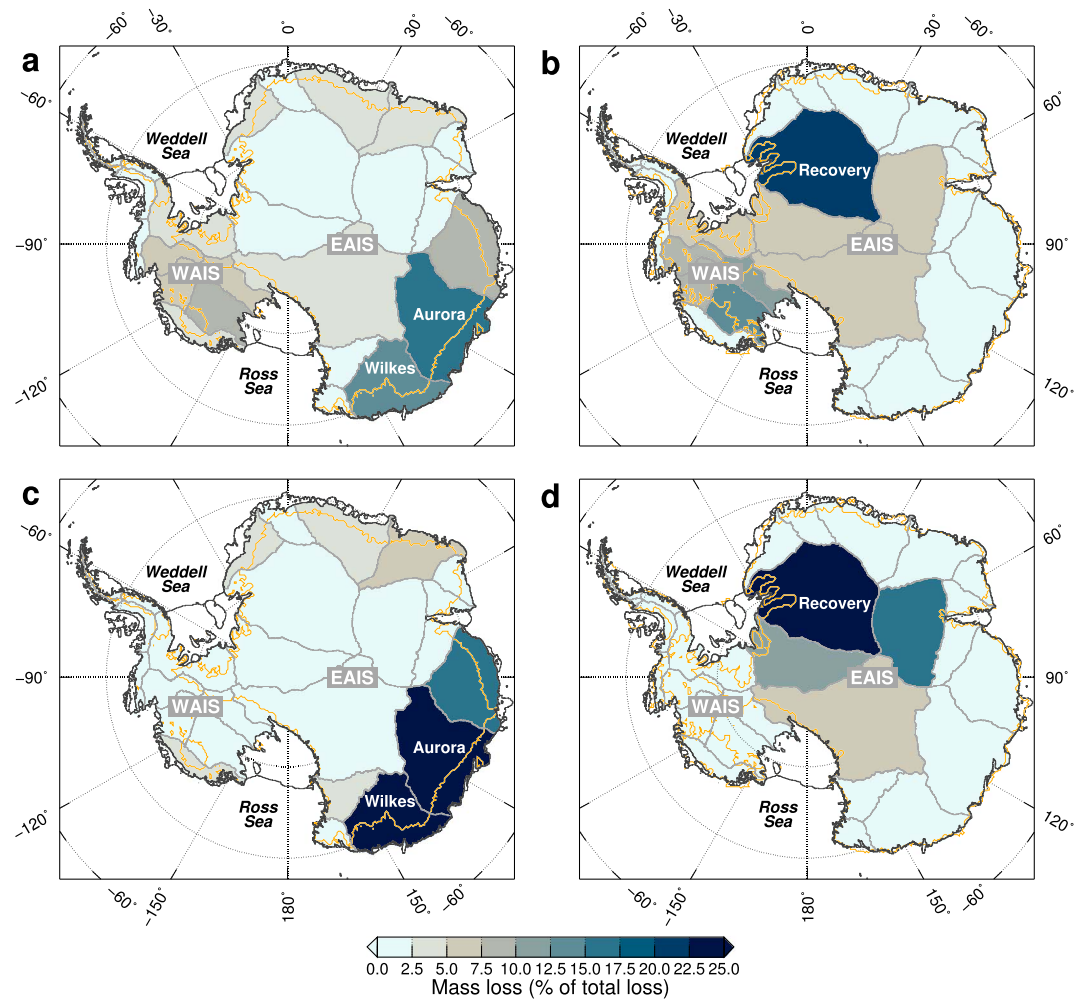
Figure 3. (a) Relative sensitivity of each Antarctic catchment to atmospheric forcing, based on the proportion of total ice loss arising with a spatially uniform air temperature increase of 8°C. Wilkes and Aurora basins exhibit by far the greatest response. (b) Relative sensitivity of Antarctic catchments to oceanic forcing, based on the proportion of total ice loss arising with a spatially uniform ocean temperature increase of 2°C. The greatest response is evident in Recovery basin. (c, d) As Figures 3a and 3b but with the ice loss effect of topography subtracted (see supporting information for details). Removing the topographic influence on ice loss highlights more clearly the spatial influence of air and ocean forcing. Orange lines denote grounding-line position at the time slice used for the mass loss calculations (10,000 years). WAIS = West Antarctic ice sheet; EAIS = East Antarctic ice sheet.

the ice margin. The magnitude of this effect is dependent on the Earth rheology parameterization and the uplift model employed; thus, different schemes may either enhance or subdue regional differences. Another limitation of our simulations is that the coarse grid resolution we employ (20 km) may underrepresent narrow subglacial troughs that could allow ingress of ocean water if grounding lines were initially destabilized. However, other studies that have employed higher-resolution, catchment-specific model domains [e.g., *Mengel and Levermann*, 2014] have also found that grounding-line retreat in the Wilkes subglacial basin can only proceed following removal of a coastal "ice plug." Our simulations present the possibility that gradual surface melting due to atmospheric warming may be one mechanism by which this plug could be removed. A final aspect of our model that differs from other whole-continent simulations is that we do not include mechanisms by which a grounded ice cliff may collapse. A model that employs such a scheme [*Pollard et al.*, 2015; *DeConto and Pollard*, 2016] produces far greater, and faster, ice margin retreat than we predict.

Consideration of these exemplar drainage basin characteristics clarifies key aspects both of the nature of catchment-scale responses to climate forcing and the topographic conditions under which such forcings may be resisted. Extending those considerations to the continent as a whole, we develop a hierarchy of vulnerability for each of the 27 Antarctic drainage basins identified from ICESat data [*Zwally et al.*, 2012]. To do this,

we calculate catchment-specific mass loss values for a scenario in which a 2°C ocean temperature anomaly is applied (without additional air temperature forcing) and one in which an 8°C air temperature anomaly is used (in the absence of additional ocean forcing). Our calculation uses present-day catchment boundaries and finds the difference in ice volume above flotation for each drainage basin at the end of the 10,000 year simulation, compared to that at initialization. Temperature values were chosen based on Climate Model Intercomparison Project phase 5 (CMIP5) long-term anomalies from present-day values for Representative Concentration Pathway (RCP) 8.5 [*Collins et al.*, 2013]. Although the length of our simulations greatly exceeds that of the CMIP5 projections, the purpose of this analysis is simply to identify spatial differences arising in response to spatially uniform forcings, and so the choice of forcing magnitude as well as the period over which it is applied is not especially important except that oceanic, and atmospheric anomalies must be sufficiently great to elicit enough of a response to enable a comparison.

Figure 3 illustrates the results of this analysis, showing mass loss arising from each catchment as a proportion of the total simulated for that scenario. The magnitude of simulated ice loss is partly a function of catchment size and partly a consequence of the length of model run, but nonetheless, the results reveal a clear spatial pattern that confirms a greater air temperature sensitivity of Wilkes and Aurora catchments compared to all other East Antarctic drainage basins. Notably, the Recovery basin catchment and its immediate neighbors exhibit much lower susceptibility to atmospheric warming of this magnitude. Conversely, when spatially uniform ocean warming is applied to the domain in the absence of atmospheric warming, the Recovery Catchment exhibits by far the greatest response of all drainage basins in Antarctica. This pattern is especially clear in the lower panels (Figures 3c and 3d) in which we subtract the volume of mass lost purely as a consequence of topographic configuration (the marine ice-sheet instability, or "MISI"; see supporting information for details [*Thomas and Bentley*, 1978; *Schoof*, 2007]). By subtracting the "pure MISI" component in this manner, the sensitivity of each sector to individual climate components can be appreciated without the topographic bias related to local bed conditions.

4. Discussion

Based on the experiments performed and described above we find that the Recovery basin catchment of East Antarctica is much more like West Antarctic drainage basins in physiography and glaciological response than other East Antarctic catchments and is more vulnerable to rising ocean temperatures than to increased air temperature. In contrast, at the spatial resolution of our simulations Wilkes and Aurora catchments are far more sensitive to warmer air temperatures and relatively insensitive to a warming ocean alone. Although our climate scenarios are idealized, we can relate the locations of the more sensitive catchments to ocean and atmosphere warming scenarios predicted by CMIP5 ensemble mean outputs for RCP 8.5. CMIP5 simulations exhibit considerable intermodel variability that is averaged out in the ensemble mean, such that regional changes (especially cooling in some areas) observed in recent decades is not evident [*Smith and Polvani*, 2016; *Turner et al.*, 2016]. This generalization notwithstanding, the ensemble mean indicates air temperature anomalies that by 2100 CE are around 4 to 5°C above preindustrial values around much of coastal East Antarctica, with higher values further inland and toward the Weddell Sea sector (Figure 4a). Ocean warming is widespread around the West Antarctic coast, but the greatest temperature anomaly occurs in the eastern Weddell Sea (Figures 4a and 4b).

Although the ocean component of the climate models does not extend beneath the extant Filchner Ice Shelf, the presence of deep submarine troughs that extend from the Weddell Sea eastward beneath the ice sheet indicates that a connectivity between the projected ocean warming and the Recovery subglacial basin is plausible (Figure 4b). Eddy-resolving ocean model simulations illustrate that ocean density gradients across the continental slope in the eastern Weddell Sea are conducive to supporting landward transport of upwelling (warm) circumpolar deep water in this region [*Stewart and Thompson*, 2015], while observations of ocean temperatures in this region are already recording pulsed incursions of wind-driven warm water [*Darelius et al.*, 2016]. This wind-driven flux of warm water into the eastern Weddell Sea is also thought to have occurred in the past and has been used to explain the apparently earlier onset of retreat in this region, compared to the rest of East Antarctica, following the Last Glacial Maximum [*Weber et al.*, 2011]. Our findings are therefore consistent with at least part of the recent geological record.

Previous modeling studies have highlighted the vulnerability of the Filchner-Ronne Ice Shelf [*Hellmer et al.*, 2012] and surrounding ice sheet [*Fogwill et al.*, 2014; *Martin et al.*, 2015; *Mengel et al.*, 2016] in varying levels
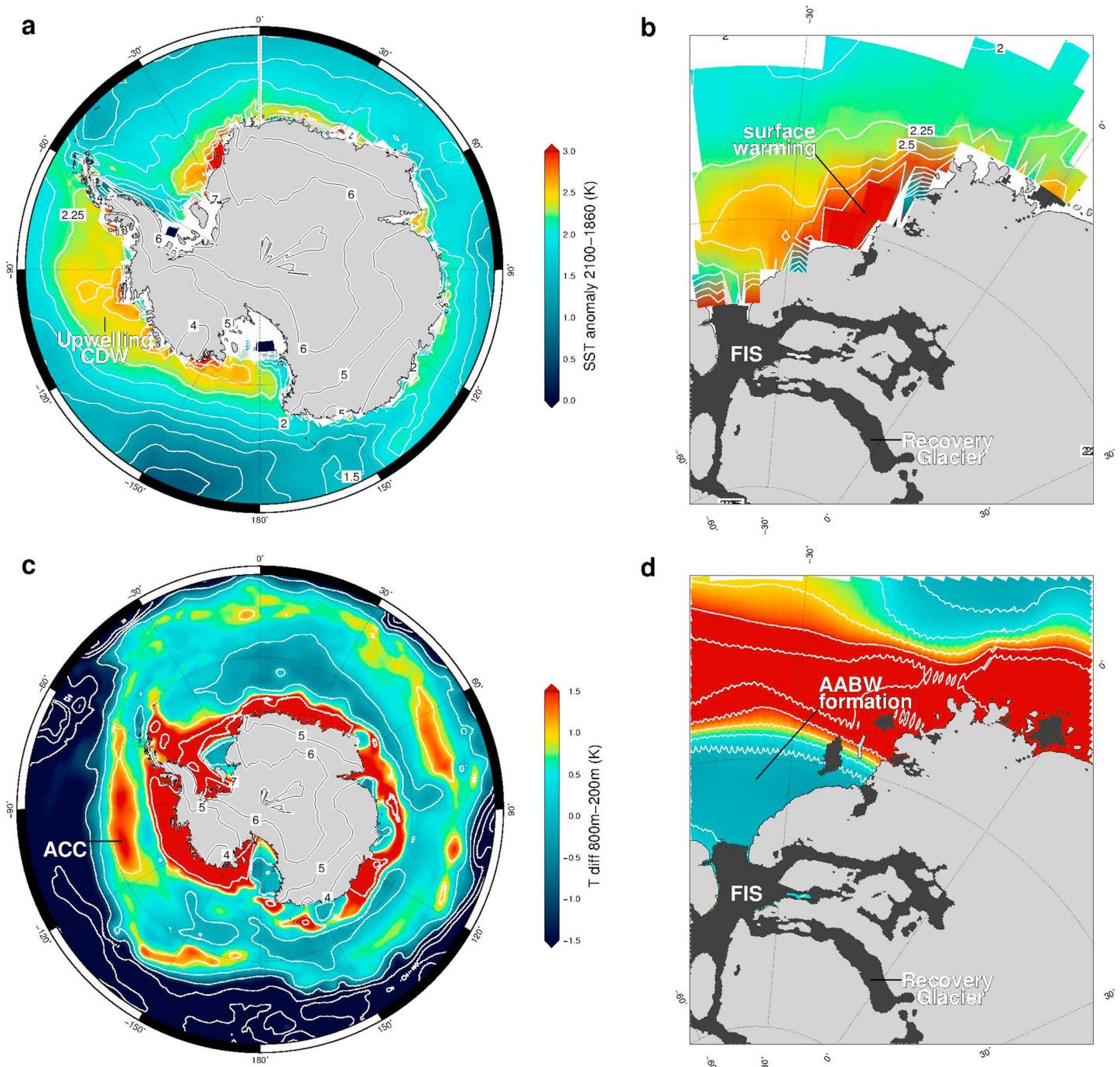
Figure 4. (a) Sea-surface temperature anomalies at 2100 CE (colored shading) with respect to preindustrial values as represented in the CMIP5 ensemble mean. Note the widespread coastal warming around West Antarctica arising from upwelling circumpolar deep water and (b) the peak warmth anomaly in the eastern Weddell Sea adjacent to the Filchner Ice Shelf (FIS). (c) Vertical ocean temperature differences revealed in World Ocean Circulation Experiment (WOCE) data. Bright colors in the Southern Ocean identify the location of the Antarctic Circumpolar Current. Areas of low thermal gradient adjacent to the continent coincide with the location of Antarctic Bottom Water formation areas, including (d) in the eastern Weddell Sea. Data shown are interpolations that fill gaps between available data points, for example, beneath ice shelves. Air temperature anomalies (in degrees C) over land shown as contours in Figures 4a and 4c. Dark gray shading in Figures 4b and 4d depicts areas of bed topography more than 500 m below sea level.

of detail; in our study we are able not only to confirm this regional sensitivity but also to establish the continental context for it (over millennial timescales) with respect to all other catchments. Furthermore, when the location of the ocean warming and the modeled sensitivity of the ice sheet in this region are considered in the context of Antarctic ocean circulation, we can see that precisely the same area of the eastern Weddell Sea is one of the few regions where Antarctic bottom water (AABW) is formed (Figures 4c and 4d). Observations elsewhere indicate that freshwater fluxes from ice melt can significantly disrupt AABW formation [*Williams et al.*, 2016], which in previous simulations we have shown to trigger a positive feedback that accelerates grounding line retreat through reduced ventilation of upwelling warm water [*Golledge et al.*, 2014]. The consequences of this feedback mechanism appear to propagate globally, leading to enhanced surface warming in the Northern Hemisphere, even for low-magnitude freshwater fluxes, due to a strengthening of the Atlantic Meridional Overturning Circulation [*Bakker et al.*, 2016].

5. Conclusions

On the basis of our experiments, previously published simulations, comparison to geological data, to present-day observations, and to CMIP5 model predictions for 2100 CE, we suggest that the majority of future ice loss from East Antarctica will most likely originate from the Recovery drainage basin in the eastern Weddell Sea. We posit that the timing and magnitude of ice sheet retreat in this area will dictate not only the East Antarctic contribution to future sea level rise but also affect the degree to which surface temperatures are amplified across the globe.

References

Aitken, A., J. Roberts, T. van Ommen, D. Young, N. Golledge, J. Greenbaum, D. Blankenship, and M. Siegert (2016), Repeated large-scale retreat and advance of Totten Glacier indicated by inland bed erosion, *Nature*, *533*, 385–389.

Bakker, P., P. U. Clark, N. R. Golledge, A. Schmittner, and M. E. Weber (2016), Centennial-scale Holocene climate variations amplified by Antarctic ice sheet discharge, *Nature*, *541*, 72–76, doi:10.1038/nature20582.

Bueler, E., and J. Brown (2009), Shallow shelf approximation as a "sliding law" in a thermomechanically coupled ice sheet model, *J. Geophys. Res.*, *114*, F03008, doi:10.1029/2008JF001179.

Collins, M., et al. (2013), Long-term climate change: Projections, commitments and irreversibility, in *Climate Change 2013: The Physical Science Basis. Contribution of Working Group I to the Fifth Assessment Report of the Intergovernmental Panel on Climate Change*, edited by M. Collins et al., pp. 1029–1136, Cambridge Univ. Press, Cambridge, U. K., and New York.

Comiso, J. (2000), Variability and trends in Antarctic surface temperatures from in situ and satellite infrared measurements, *J. Clim.*, *13*(10), 1674–1696.

Darelius, E., I. Fer, and K. W. Nicholls (2016), Observed vulnerability of Filchner-Ronne ice shelf to wind-driven inflow of warm deep water, *Nat. Commun.*, *7*, 12300, doi:10.1038/ncomms12300.

DeConto, R., and D. Pollard (2016), Contribution of Antarctica to past and future sea-level rise, *Nature*, *531*, 591–597.

Feldmann, J., T. Albrecht, C. Khroulev, F. Pattyn, and A. Levermann (2014), Resolution-dependent performance of grounding line motion in a shallow model compared to a full-Stokes model according to the MISMIP3d intercomparison, *J. Glaciol.*, *60*, 353–360.

Fogwill, C. J., C. S. Turney, K. J. Meissner, N. R. Golledge, P. Spence, J. L. Roberts, M. H. England, R. T. Jones, and L. Carter (2014), Testing the sensitivity of the East Antarctic ice sheet to Southern Ocean dynamics: Past changes and future implications, *J. Quat. Sci.*, *29*(1), 91–98.

Fretwell, P., et al. (2013), Bedmap2: Improved ice bed, surface and thickness datasets for Antarctica, *The Cryosphere*, *7*(1), 375–393.

Frieler, K., P. U. Clark, F. He, C. Buizert, R. Reese, S. R. Ligtenberg, M. R. van den Broeke, R. Winkelmann, and A. Levermann (2015), Consistent evidence of increasing Antarctic accumulation with warming, *Nat. Clim. Change*, *5*, 348–352.

Golledge, N., L. Menviel, L. Carter, C. Fogwill, M. England, G. Cortese, and R. Levy (2014), Antarctic contribution to meltwater pulse 1A from reduced Southern Ocean overturning, *Nat. Commun.*, *5*, 1–10, doi:10.1038/ncomms6107.

Golledge, N., D. Kowalewski, T. Naish, R. Levy, C. Fogwill, and E. Gasson (2015), The multi-millennial Antarctic commitment to future sea-level rise, *Nature*, *526*, 421–425.

Golledge, N. R., Z. A. Thomas, R. H. Levy, E. G. W. Gasson, T. R. Naish, R. M. McKay, D. E. Kowalewski, and C. J. Fogwill (2016), Antarctic climate and ice sheet configuration during a peak-warmth early Pliocene interglacial, *Clim. Past Discuss.*, doi:10.5194/cp–2016–123, in press.

Hellmer, H., S. Jacobs, and A. Jenkins (1998), Oceanic erosion of a floating Antarctic glacier in the Amundsen Sea, in *Ocean, Ice, and Atmosphere: Interactions at the Antarctic Continental Margin*, edited by S. Jacobs and R. Weiss, pp. 75–319, Antarctic Research Series, AGU, Washington D. C.

Hellmer, H., F. Kauker, R. Timmermann, J. Determann, and J. Rae (2012), Twenty-first-century warming of a large Antarctic ice-shelf cavity by a redirected coastal current, *Nature*, *485*, 225–228.

Holland, D. M., and A. Jenkins (1999), Modeling thermodynamic ice-ocean interactions at the base of an ice shelf, *J. Phys. Oceanogr.*, *29*, 1787–1800.

Lenaerts, J., M. van den Broeke, W. van de Berg, E. van Meijgaard, and P. Munneke (2012), A new, high-resolution surface mass balance map of Antarctica (1979–2010) based on regional atmospheric climate modeling, *Geophys. Res. Lett.*, *39*, L04501, doi:10.1029/2011GL050713.

Martin, M. A., A. Levermann, and R. Winkelmann (2015), Comparing ice discharge through West Antarctic Gateways: Weddell vs Amundsen Sea warming, *Cryosphere Discuss.*, *9*(2), 1705–1733.

Mengel, M., and A. Levermann (2014), Ice plug prevents irreversible discharge from East Antarctica, *Nat. Clim. Change*, *4*, 451–455.

Mengel, M., J. Feldmann, and A. Levermann (2016), Linear sea-level response to abrupt ocean warming of major West Antarctic ice basin, *Nat. Clim. Change*, *6*, 71–74.

Pollard, D., R. M. DeConto, and R. B. Alley (2015), Potential Antarctic Ice Sheet retreat driven by hydrofracturing and ice cliff failure, *Earth Planet. Sci. Lett.*, *412*, 112–121.

Rignot, E., J. Mouginot, and B. Scheuchl (2011), Ice flow of the Antarctic ice sheet, *Science*, *333*, 1427–1430.

Rintoul, S. R., A. Silvano, B. Pena-Molino, E. van Wijk, M. Rosenberg, J. S. Greenbaum, and D. D. Blankenship (2016), Ocean heat drives rapid basal melt of the Totten Ice Shelf, *Sci. Adv.*, *2*(12), E1601610, doi:10.1126/sciadv.1601610.

Ritz, C., T. L. Edwards, G. Durand, A. J. Payne, V. Peyaud, and R. C. Hindmarsh (2015), Potential sea-level rise from Antarctic ice-sheet instability constrained by observations, *Nature*, *528*, 115–118.

Rogozhina, I., and D. Rau (2014), Vital role of daily temperature variability in surface mass balance parameterizations of the Greenland Ice Sheet, *The Cryosphere*, *8*, 575–585.

Schoof, C. (2006), A variational approach to ice stream flow, *J. Fluid Mech.*, *556*, 227–251, doi:10.1017/S0022112006009591.

Schoof, C. (2007), Ice sheet grounding line dynamics: Steady states, stability, and hysteresis, *J. Geophys. Res.*, *112*, F03S28, doi:10.1029/2006JF000664.

Seguinot, J. (2013), Spatial and seasonal effects of temperature variability in a positive degree-day glacier surface mass-balance model, *J. Glaciol.*, *59*, 1202–1204.

Smith, K. L., and L. M. Polvani (2016), Spatial patterns of recent Antarctic surface temperature trends and the importance of natural variability: Lessons from multiple reconstructions and the CMIP5 models, *Clim. Dyn.*, 1–18, doi:10.1007/s00382-016-3230-4.

Stewart, A. L., and A. F. Thompson (2015), Eddy-mediated transport of warm Circumpolar Deep Water across the Antarctic shelf break, *Geophys. Res. Lett.*, *42*(2), 432–440, doi:10.1002/2014GL062281.

Thomas, R. H., and C. R. Bentley (1978), A model for Holocene retreat of the West Antarctic Ice Sheet, *Quat. Res.*, *10*(2), 150–170.

Turner, J., H. Lu, I. White, J. C. King, T. Phillips, J. S. Hosking, T. J. Bracegirdle, G. J. Marshall, R. Mulvaney, and P. Deb (2016), Absence of 21st century warming on Antarctic Peninsula consistent with natural variability, *Nature*, *535*(7612), 411–415.

Weber, M. E., P. U. Clark, W. Ricken, J. X. Mitrovica, S. W. Hostetler, and G. Kuhn (2011), Interhemispheric ice-sheet synchronicity during the Last Glacial Maximum, *Science*, *334*, 1265–1269.

Williams, G., et al. (2016), The suppression of Antarctic bottom water formation by melting ice shelves in Prydz Bay, *Nat. Commun.*, *7*, 12577.

Winkelmann, R., M. A. Martin, M. Haseloff, T. Albrecht, E. Bueler, C. Khroulev, and A. Levermann (2010), The Potsdam Parallel Ice Sheet Model (PISM-PIK)—Part 1: Model description, *The Cryosphere*, *5*, 715–726.

Zwally, H. J., M. B. Giovinetto, M. A. Beckley, and J. L. Saba (2012), Antarctic and Greenland Drainage Systems, GSFC Cryospheric Sci. Lab. [Availbale at http://icesat4.gsfc.nasa.gov/cryo_data/ant_grn_drainage_systems.php.]